University of Texas Rio Grande Valley

ScholarWorks @ UTRGV

5-2021

Topologically Robust Bulk State in Non-Hermitian Acoustic System

Jannatul Ferdous
The University of Texas Rio Grande Valley

Follow this and additional works at: https://scholarworks.utrgv.edu/etd

Part of the Physics Commons

Recommended Citation

TOPOLOGICALLY ROBUST BULK STATE IN NON-HERMITIAN ACOUSTIC SYSTEM

A Thesis

by

JANNATUL FERDOUS

Submitted to the Graduate College of
The University of Texas Rio Grande Valley
In partial fulfillment of the requirements for the degree of

MASTER OF SCIENCE

May 2021

Major Subject: Physics

TOPOLOGICALLY ROBUST BULK STATE IN NON-HERMITIAN ACOUSTIC SYSTEM

A Thesis
by
JANNATUL FERDOUS

COMMITTEE MEMBERS

Dr. Hamidreza Ramezani
Chair of Committee

Dr. Ahmed Touhami
Committee Member

Dr. Cem Yuce
Committee Member

May 2021

ABSTRACT

Ferdous, Jannatul, <u>Topologically robust bulk state in non-Hermitian acoustic system</u>. Master of Science (MS), May, 2021, 45 pp., 15 figures, references, 36 titles.

Topological aspects can be observed in different types of models or structures. Among them the 1D Su-Schrieffer-Heeger (SSH) Model is a very convenient one where we observe the zero-mode energy state with localized mode profile generated in the structure at the interface of two topologically distinct structures. These distinct structures are so called trivial and non-trivial topological structures. This type of zero mode is known as edge state as it forms at the edge and demonstrates topological robustness against defects or disorders. If we add gain, loss or disorder in the system in such a way that the topology of the system does not change, and the symmetry is protected, and keeping the topology robust under such disorder we can see many exotic phenomena in both optics and acoustics, like the phenomenon of disorder-free one-way sound propagation, which does not occur in typical acoustic devices. Whereas a trivial topological insulator only allows topologically robust edge state, we investigate another type of one-dimensional lattice where topologically robust bulk state is observed, which can pave a way to robust transport of acoustic signal through the bulk. In this thesis we will theoretically explore the behavior of such a system as well as demonstrate our numerical and experimental findings to support our claims. We will also demonstrate how we built a tunable non-Hermitian acoustic filter by adjusting the non-Hermiticity in the system and show how experimental data verifies simulation.

DEDICATION

To my Family members, Teachers and friends who were always there for me in good and bad times and always encouraged me to be the best version of myself.

ACKNOWLEDGMENTS

My special and sincere thanks to my supervisor, Dr. Hamidreza Ramezani, for the patient guidance, encouragement, and advice he has provided throughout my research and beyond.

Then, I would like to thank my family members for not giving up on me and specially my husband, Nageeb Zaman for supporting and encouraging me through my struggles.

I would also like to thank my thesis committee members Dr Ahmad Touhami and Dr. Cem Yuce for being in my thesis committee.

Thanks to my Lab mate Sandeep Puri for being a such good research partner.

And last but not the least, I want to thank the faculty members and staffs of the UTRGV physics department for their support whenever it was needed, specially Dr. Soma Mukherjee for her help and recommendations for my PhD application.

TABLE OF CONTENTS

LIST OF FIGURES

ix

CHAPTER I

INTRODUCTION

1.1 Hermitian and Non-Hermitian Systems:

The development of quantum mechanics is a little over hundred years old which started with theoretical predictions. As there have been so many experimental verifications of its theoretical predictions, it has become an established and accepted component of modern science. There are fundamental postulates characterizing the theory which need physical verifications. However, there is one postulate that stands out because it is mathematical rather than physical in character, which requires a Hamiltonian operator(Witte, 2009), expressing the dynamics of the quantum system to be Hermitian and it dates back to the early days of quantum mechanics. The Hermiticity of H is expressed by the equation:

$$H = H^{\dagger}$$

Here the symbol $\dagger$ represents the combined operations of matrix transposition and complex conjugation. Despite the physical obscurity of this mathematical symmetry condition it is very convenient because it implies that the eigenvalues of H are real and that the time-evolution

1

operator e^{-iHt} is unitary and the Hermitian Hamiltonian conserves probability namely the norm of a state. These eigenvalues correspond to some observables, as they are the potential outcomes of measurements(Bender, 2007).

In conventional quantum mechanics, a closed or isolated system is one with no interaction with the environment, evolves according to a Hermitian Hamiltonian. This so-called closed system is considered to be idealized because its time evolution experiences no influence by the external environment. It is not possible to observe a closed system in a laboratory because making a measurement requires that the system be in contact with the external world. Physically realistic systems, such as scattering experiments, are open systems, which are called non-Hermitian systems(Bender, 2007). Such type of system experiences transfers of energy from/to the outside world. This type of open dissipative systems can be created introducing gain/loss mechanism in a system associated with Hermitian Hamiltonian.

Non-Hermitian Hamiltonian operators, H_N (for $H_N \neq H_N{}^\dagger$) have been proved useful in describing loss/gain mechanisms, open systems, phenomenon of radioactive decay and dephasing(Ashida et al., 2020). While the NH version of quantum mechanics is helpful in simplifying calculations and for identifying resonances, the assumption has long been that NH operators are not physically meaningful, because these non-Hermitian Hamiltonians are only approximate, phenomenological descriptions of physical processes. They cannot be regarded as fundamental because they violate the requirement of unitarity. Decades ago this assumption was shown to be wrong, when researchers found that the observables of certain Non-Hermitian operators that obey combined parity time (PT)-reversal symmetry (for $H_N = H_N{}^{PT}$) exhibits the

real eigenvalues or energy spectrum(Schindler et al., 2012). It took a decade for these concepts to be introduced into acoustics(Ramezani et al., 2012).

1.2   Concept of Topology:

Topology is a branch of math where we study shapes. It is the mathematical study of the properties that are preserved through deformations, twisting, and stretching of objects. Tearing, however, is not allowed. To understand that we need to concentrate on [Figure 1.1 (a)] and imagine the donut

(a)   (b)

(c)
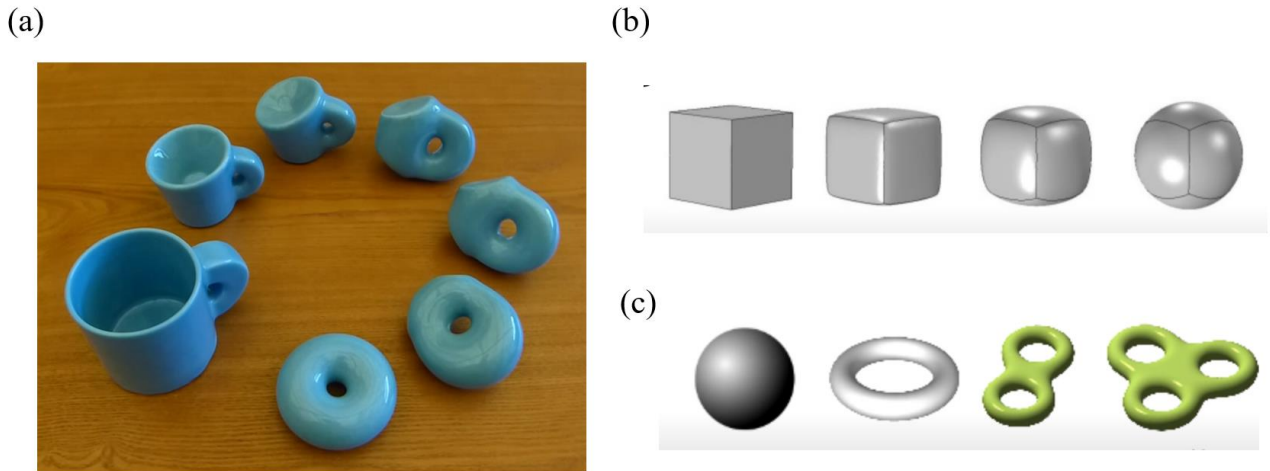
Figure 1. 1: (a) Deformation of a coffee mug into a donut without changing the topology. (b) deformation of a hollow cube into a sphere without changing the topology. (c) objects with different holes have different topology.

made out of clay(*Topology in Physics*, n.d.). It's possible to stretch the clay in a continuous manner so that it ends up as a coffee mug permitting that we don't cut or glue any clay we started with. We can perform such an action as they have the same topology. Similarly, we can change

3

the cube [Figure 1.1 (b)] into a sphere by similar deformation, without cutting or gluing. In [Figure 1.1 (c)] we can see several objects and they have different topology because of existence of different number of holes in the structure(Billie Eilish, 2015).

This is the natural fundamental mathematical property of any object, which is being investigated in many different areas from mathematics to physics and engineering. Topological phases(Moessner & Moore, 2021) of Hermitian systems are known to exhibit intriguing properties such as the presence of robust localized edge states and the famed bulk-boundary correspondence. These features can change drastically for their non-Hermitian generalizations. The application of topology in optics has led to a new paradigm in developing photonic devices with robust properties against disorder. Acoustic technologies have frequently developed in tandem with optics, using shared concepts such as waveguiding and meta-media. The electronic edge states have been demonstrated occurring in topological insulators(Hasan & Kane, 2010) and possess a striking and technologically promising property: the ability to travel in a single direction along a surface without back-scattering(Svela et al., 2020), regardless of the existence of defects or disorder. The phenomenon of disorder-free one-way sound propagation, which does not occur in ordinary acoustic devices, may have novel applications for acoustic isolators(Yang et al., 2015), ultrafast modulators(Zhao et al., 2015), and transducers.

1.3   Bloch's theorem in Periodic lattice:
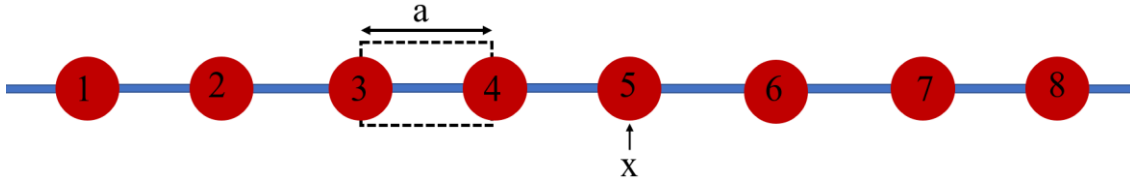
Figure 1. 2: One dimensional periodic lattice with lattice constant a and 8 sites.

Bloch's theorem is usually used in many disciplines like quantum mechanics, Electricity and Magnetism, Solid State Physics that rely on periodicity. The very known example of Bloch's theorem is describing electrons in a crystal, especially in characterizing the crystal's electronic properties(Jamuna TV, 2019). However, it can also describe the symmetry property of a periodic dielectric structure in electromagnetism leads to photonic crystals, and a periodic acoustic medium leads to phononic crystals/ acoustic metamaterials("Acoustic Metamaterial," 2021). To understand what we mean by the symmetry of crystals, we will consider a one-dimensional infinite array of atoms, sites, or potentials [Figure 1.2].

Consider a one-dimensional lattice with lattice constant a. If we consider the position of 5th site to be x, 6th site to be $(x + a)$, 4th site to be $(x - a)$ and so forth and if we want to know the probability of finding the wave function in each site of this infinite crystal we will find the probability relation like bellow,

$$|\psi(x)|^2 = \ |\psi(x + a)|^2 = |\psi(x - a)|^2$$

And the wavefunctions at different sites are related by

$$\psi(x + a) = c.\psi(x) \quad or \quad \psi(x) = c.\psi(x - a)$$

As the magnitude of coefficient c, |c|=1. We know a function whose magnitude is always 1 which is e^{ikx} .

      To find the other possible values of c, we use periodic boundary conditions on that infinite lattice by adding one end of the lattice with the other assuming that the crystal lattice has the form of a circle [Figure 1.3]. To clarify the idea, we need to do an approximation. The approximation is that if it was a finite lattice, it would end up as a figure like [Figure 1.2]. But if this was an infinitely large circle it would look like a straight line of atom. So, this argument is only valid for infinite crystals with $N=\infty$ number of atoms or sites, which leads us to the relation, considering [Figure 1.3] (where $N=8$)

$$\psi(x + Na) = c.\psi(x) = c^8.\psi(x)$$

We also expect the condition to be $c^N.\psi(x) = \psi(x)$ as c^N should be equal to 1.

So, $c = \sqrt[N]{1} = e^{i2\pi s/N}$, where s=1, 2, 3, 4, 5, …, N.
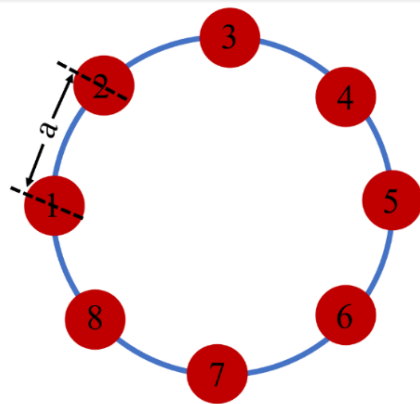
Figure 1. 3 Approximated circular lattice after applying periodic boundary condition.

Now we need to figure out the wave function $\psi(x)$ by putting the value of c.

$$\psi(x + a) = e^{i2\pi s/N} . \psi(x)$$

And eventually we get the wave function

$\psi(\mathrm{x}) = e^{i2\pi s/N.x/a}$ where wave vector, $k = 2\pi s/N.a$

$$= e^{ikx} u_k(x)$$

where $u_k(x)$ is a periodic function with the same periodicity as the lattice. Which is the statement of Bloch's theorem in a periodic lattice(Jamuna TV, 2019). Unlike Hermitian lattices, periodic and open boundary conditions in non-Hermitian lattices can have drastically different spectra. In non-Hermitian systems, non-Bloch band theory has recently been developed.

1.4   Spring mass model:

We can also apply this periodicity conditions in a spring mass model [Figure 1.4]. Similar to [Figure 1.2], if we consider a one-dimensional lattice with N number of masses or sites are attached to each other by springs with spring constant or coupling t, and the whole system acts as a coupled oscillator(Thorton & Marion, n.d.). If the wavefunction corresponds to each mass is,

$$\psi(\mathrm{x}) = C\, e^{-\alpha x^2},$$

where $\alpha = \frac{\sqrt{tm}}{2\hbar}$, and C is the amplitude of probability that the acoustic wave function is localized at mass n.
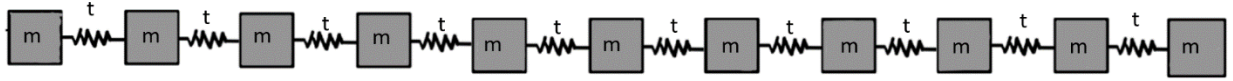
Figure 1. 4 One dimensional spring mass lattice, cubes are with mass $m_1, m_2, ...m_{11}$ for 11 sites. t is the coupling strength between the sites.

Here, mass, m = m_1 = m_2 = m_3=...m_7(*Quantum Harmonic Oscillator*, n.d.). If all the same masses are connected by the springs with same spring constant t, then the equation of motion for the masses of the spring mass system Figure 1.4 writes,

$$m\frac{d^2x_n}{dt^2} = - t\ (2x_n - x_{n+1}\ ),$$ for first mass from left in Figure 1.4

$$m\frac{d^2x_n}{dt^2} = - t\ (2x_n - x_{n-1}- x_{n+1}\ ),$$ for middle masses

$$m\frac{d^2x_n}{dt^2} = - t\ (2x_n - x_{n-1}\ ),$$ for last mass from left in Figure 1.4(Thorton & MArion, n.d.)

In this thesis we have proposed a 1D lattice model similar to this mass spring model where the Hamiltonian H, associated with the system that we are talking about is a non-invertible Hamiltonian, which means the inverse of the Hamiltonian H^{-1} does not exist. The important properties of this Hamiltonian are it is a singular square matrix, the determinant of it is zero, *Det[H] = 0* and we get zero energy eigenvalue with a nonzero energy eigenstate (C. Yuce, 2019.).

CHAPTER II

NUMERICAL AND EXPERIMENTAL OBSERVATION OF TOPOLOGICALLY ROBUST
STATES

2.1 General outlook on topologically robust state:

The concept of topological order has recently inspired scientists working in many branches

of physics and engineering to look for topologically nontrivial states in several fields of interest.

This concept was originally discovered in condensed matter physics. In condensed matter,

topological states of matter are inherently related to the symmetry property of structure.

Topological robustness is a property of a structure, lattice, or system. It can be checked if a

system possesses this quality by introducing defects in a Hermitian system when symmetry is

protected in that system.

2.2 Topologically robust localized edge state:

To demonstrate how we observe topologically robust bulk state we will discuss the

conventional model that distinguishes the trivial and non-trivial topological system and the

appearance of zero mode in such type of system which are specially localized and robust under

deformation(C. Yuce, n.d.). Let us consider a spring and mass model. In this model, first consider the case where the spring constant $k_1 > k_2$. We are calling it trivial case [Figure 2.1 (a)]. These spring constants refers to the coupling between the masses. As the coupling k_1 is larger than the coupling k_2, every pair of masses with stronger coupling are forming a dimer. Here, we can also calculate the eigenvalues or eigenfrequencies associated with this structure which is shown in [Figure 2.1 (c)]. Here we can see that these two bands, they are separated by a gap. This gap is associated with the hole that we discussed before in the first chapter.

Now, to change the trivial structure to a non-trivial one we will gradually decrease and increase k_1 and k_2 respectively, and at some point, we will reach $k_2 > k_1$. This new structure will be called non-trivial structure(Zangeneh-Nejad & Fleury, 2019). In the non-trivial system, we can see that the dimerization forms between 2nd and 3rd mass, and there are two masses at two edges which are alone. If we look at the band structure in [Figure 2.1 (d)], we can see two zero-energy states corresponding to these masses who are sitting alone. These two zero modes are so called topologically robust edge state. They are called edge states because if we look at the corresponding eigenvector, we can see that the eigenvector is exponentially localized around edges of the system [Figure 2.1 (f)] and is observed at the interface of two different lattices (trivial → air medium, and non-trivial → spring-mass lattice). Now if we apply disorder in the system, i.e. if we change the coupling by a small percentage randomly, we find the [Figure 2.1 (e)] where it is clearly visible that the points on the bulk have moved by certain amount, but the

zero modes correspond to the lone masses stay at the same frequency, and the associated

eigenvector plot [Figure 2.1 (g)] shows the similar localized edge state.
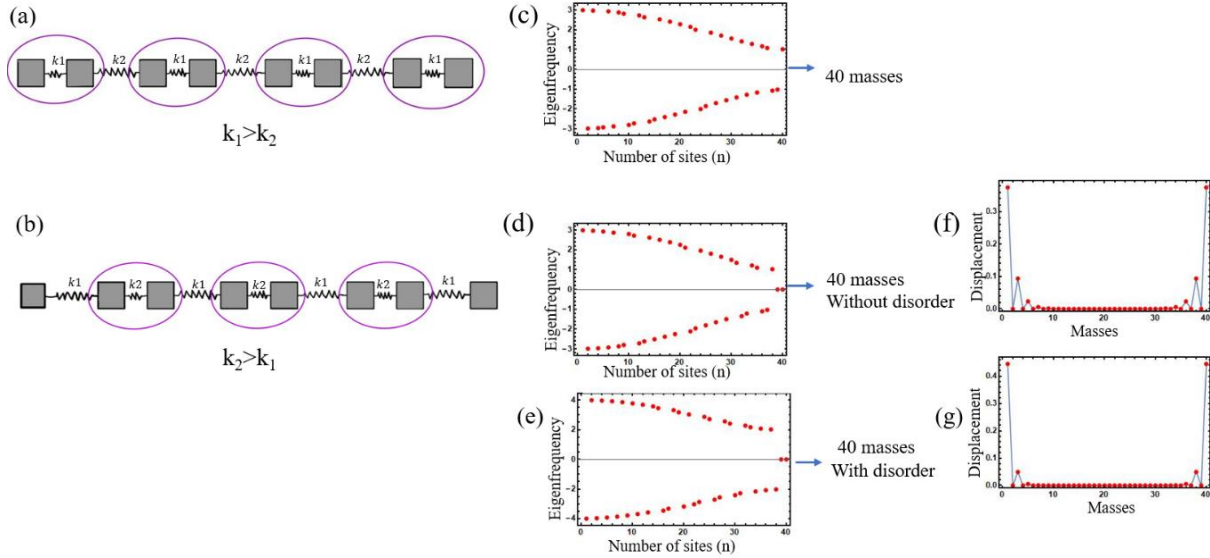
Figure 2. 1: (a)Trivial mass spring system when coupling k1>k2. (b) non-trivial mass spring system when coupling k2>k1, (c), (d) Eigenfrequency plot/band structure for (a) and (b) respectively, (e) Band structure for a system after applying disorder in (b), (f) & (g) are the eigenvector plots associated with (d) & (e) respectively.

So, it confirms the topologically robust edge state(Gao et al., 2020), but the bulk states seem

to fluctuate from their original position. We also observe this type of robustness in topological

insulator(Qi & Zhang, 2011). Topological insulators do not allow conduction in the bulk, yet

they support edge modes that travel along the boundary only in one direction, with inherent

robustness to defects and disorder.

11

2.3 Formalism of topologically robust bulk state:

In the previous section, we have seen that these edges zero modes are robust against disorder. Now the question is: Can we have a system where the bulk states can be robust? The answer is Yes. We propose an acoustic model where we claim that under certain conditions, we can have zero modes for robust bulk state, which is not localized but an extended state(Rivero & Ge, 2020).

The proposed acoustic model is associated with a non-invertible Hamiltonian. After building the Hamiltonian of the system in Figure 1.4 we can also plot the eigenfrequencies as well as eigenvectors for this system. The matrix of the corresponding the spring mass lattice with 5 sites which is equivalent to the matrix of our proposed acoustic model:

$$\begin{bmatrix} 2t - m\omega^2 & t & 0 & 0 & 0 \\ t & 2t - m\omega^2 & t & 0 & 0 \\ 0 & t & 2t - m\omega^2 & t & 0 \\ 0 & 0 & t & 2t - m\omega^2 & t \\ 0 & 0 & 0 & t & 2t - m\omega^2 \end{bmatrix}$$

It helps us to find the eigenvalue for our system. We know in non-invertible Hamiltonian the determinant is zero and we get zero energy eigenstate, which we can see in the energy diagrams of [Figure 2.2 (a),(c),(e)], and which is situated in the bulk. For this system with non-invertible Hamiltonian, the coupling among the masses are same and all the objects are of same mass, we

observe extended states like corresponding [Figure 2.2 (b),(d),(f)], to the zero energy eigenstate (Shulman & Prodan, 2010).

[Figure 2.2 (a) & (b)] correspond to the system with no loss and disorder. [Figure 2.2 (a)] shows the band diagram for a system with 41 sites and the eigenfrequencies corresponding to each site is also shown. [Figure 2.2 (b)] demonstrates the eigenmode of the system associated with the zero eigenfrequency. [Figure 2.2 (c), (d), (e), (f)] display the same information, whereas [Figure 2.2 (c) & (d)] are for a system with random disorder, but no loss and [Figure 2.2 (e) & (f)] are for a system with random disorder and certain loss. Here, it can be easily observed that after applying disorder and loss in the system the shape of the eigenmodes are changing, while keeping the zero eigenfrequency unperturbed, which is a clear indication of topological robustness of the system for a particular eigenfrequency. It is also visible that this eigenmode associated with the zero eigenfrequency is sitting in the band (bulk). Another important aspect of topological modes is that they are known to be protected by some symmetries. The symmetry of our system is followed by the Bloch's theorem which we have discussed in chapter I(Jamuna TV, 2019).

To make the same Hamiltonian invertible we need to use objects with different masses that are coupled together. Instead of non-invertible Hamiltonian if we worked with an invertible one, we could still get the robust bulk state. If this new invertible Hamiltonian shares simultaneous zero energy eigenstate with the former non-invertible one, then we will see a robust bulk extended state associated with non-zero energy eigenstate for our new invertible Hamiltonian(C. Yuce, n.d.).
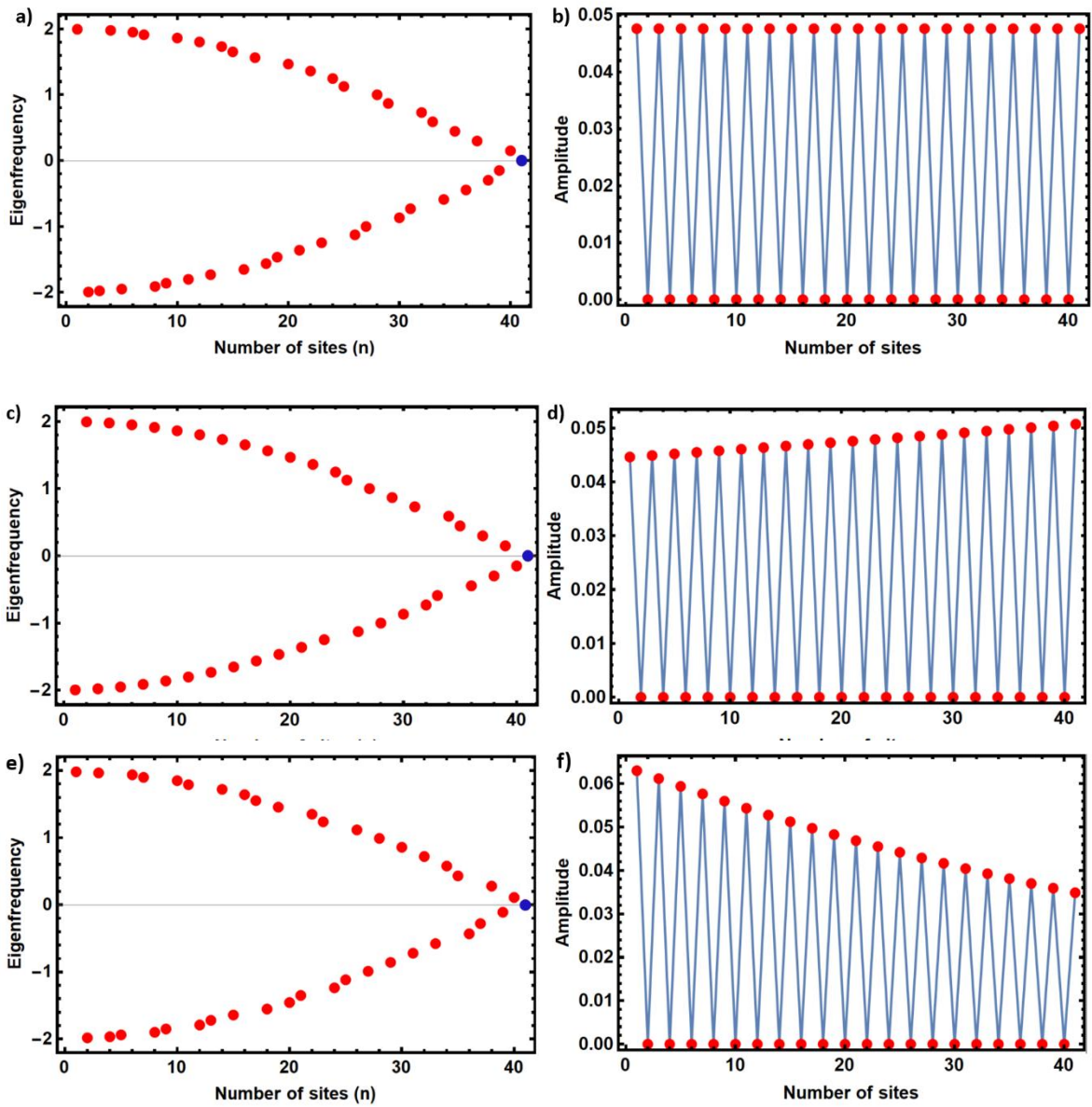
Figure 2. 2: Eigenfrequency and eigenvector diagrams for a mass spring lattice with 41 sites. Eigenfrequency and eigenvector diagrams (a), (b), when there is no disorder and no loss in the system, (c), (d), when there is random disorder but no loss, (e), (f), when there is random disorder with certain loss.

Considering the lattice constant of the structure to be *a*, the wave functions for different position in the periodic acoustic lattice becomes $\psi(x)$, $\psi(x + a)$, $\psi(x + 2a)$, $\psi(x + 3a)$,...$\psi(x + na)$. According to Bloch's theorem,

$$\psi(x + a) = e^{ika}\psi(x)$$

After applying the symmetry operator n times, it becomes,

$$\psi(x + a) = e^{ikna}\psi(x)$$

which tells us that the wavefunction looks just like a plane wave provided we only look at identical points within the unit cell (points differing by a distance that is an integer multiple of the lattice constant *a*.

Following our initial observation, we propose a realistic acoustic model and build it using COMSOL MULTIPHYSICS(*COMSOL*, n.d.) software [Figure 2.3], where we achieve this topologically robust bulk state. This is a two-port hollow wave guide where the cuboids are connected by the rectangles, in a way it can be said that the rectangles are acting as the coupling strength between the cuboids. As the acoustic wave sent into the waveguide is airborne(Al Jahdali & Wu, 2018), the density and bulk modulus of the air plays a very important role in controlling the scattering parameters for the acoustic signal. The density of the air, $\rho = 1.4$ Kg/m^3 and the effective bulk modulus, $B = 0.931 \times 10^5 (1 + 0.01i)$ Pa. The positive imaginary part in the bulk modulus is an indication of loss in the system. Though our proposed system is a Hermitian system, because of some unintentional induced loss in the system we get the imaginary part in the bulk modulus. It indicates that if we apply this physics in a device with a little interaction with environment the topological robustness will still there(Shulman & Prodan, 2010).

2.4 Proposed realistic acoustic model
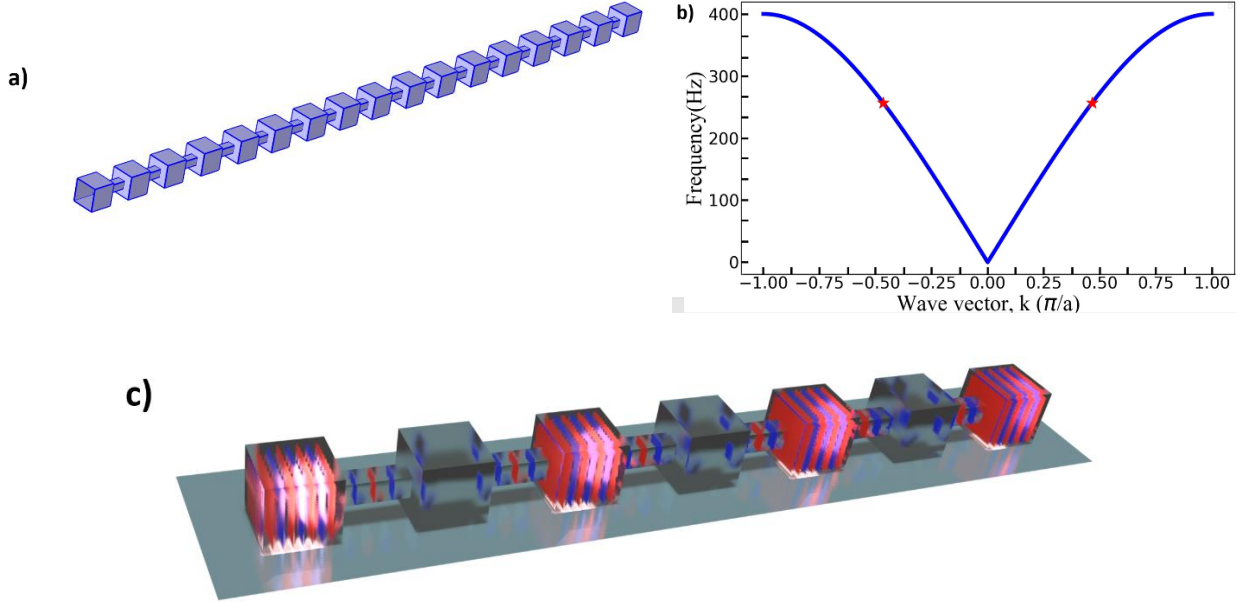
Figure 2. 3: Schematic of realistic acoustic model. (a) show a waveguide with 17 cuboids (with dimension 7×7×7 cm^3) connected by 16 rectangles (with dimension 2.3×2.3×7 cm^3). (b) demonstrates the corresponding band structure for the waveguide. (c) shows the realistic visualization of the mode profile of the waveguide at eigenfrequency 257.15 Hz, which is a robust bulk mode. two blue start in the band structure in (b) refers to the frequency 257.17 Hz which situates in the band (bulk).

In [Figure 2.3 (b)] the red band is the corresponding band structure of our periodic waveguide in [Figure 2.3 (a)], where at frequency 257.15 Hz (along the blue start marks in the band) we observe the topologically robust bulk state, which supports the underlying idea of our proposal that we find the topological protection against disorder for a certain eigenfrequency of the system which situates in the band. Figure 2.3 (c) displays the similar shape of eigenmode that

we expected for the structure in [Figure 2.3 (a)] at eigenfrequency 257.15 Hz. For the sake of convenience, we used 7 cuboids instead of 17 cuboids, yet both are odd numbers, which is a matter of concern here.

2.5 Numerical observation of topologically robust bulk state:

The geometry of the waveguide analyzed in our model is depicted in [Figure 2.3 (a)]. We apply port boundary conditions at the inlet and outlet while simulating the transmission spectrum (Zangeneh-Nejad & Fleury, 2019). We burst the left end of the waveguide with input acoustic signal and the transmitted output signal is measured at the right end. What we can observe here is that all the cuboids located at the odd numbered position experience high pressure field (cuboids with both blue and red colored field surfaces indicate high pressure) and the cuboids located at the even numbered position experience low pressure field (cuboids with only both blue colored field surfaces indicate low pressure). This mode shape is very much like what we see in [Figure 2.2 (b), (d), (f)]. There odd numbered sites have high amplitudes and even numbered sites have low amplitude (which is zero here) In [Figure 2.4] three transmission spectrums are portrayed where blue curve is the system without any disorder, and red and green curves are both with certain disorder. For all these systems the eigen-frequencies situate at the peaks of the curves. For the first peak, if we consider all three systems, we will see the eigen frequencies for blue curve lies at 229.26 Hz, for red curve at 229.80 Hz and for green curve at 230.91 Hz. For the second peak the eigen frequencies for blue curve lies at 257.2 Hz, for red curve at 256.9 Hz and for green curve at 257.01 Hz. Similarly, for the third peak, the eigen frequencies for blue curve lies at 283.1 Hz, for red curve at 282.2 Hz and for green curve at 281.5 Hz.
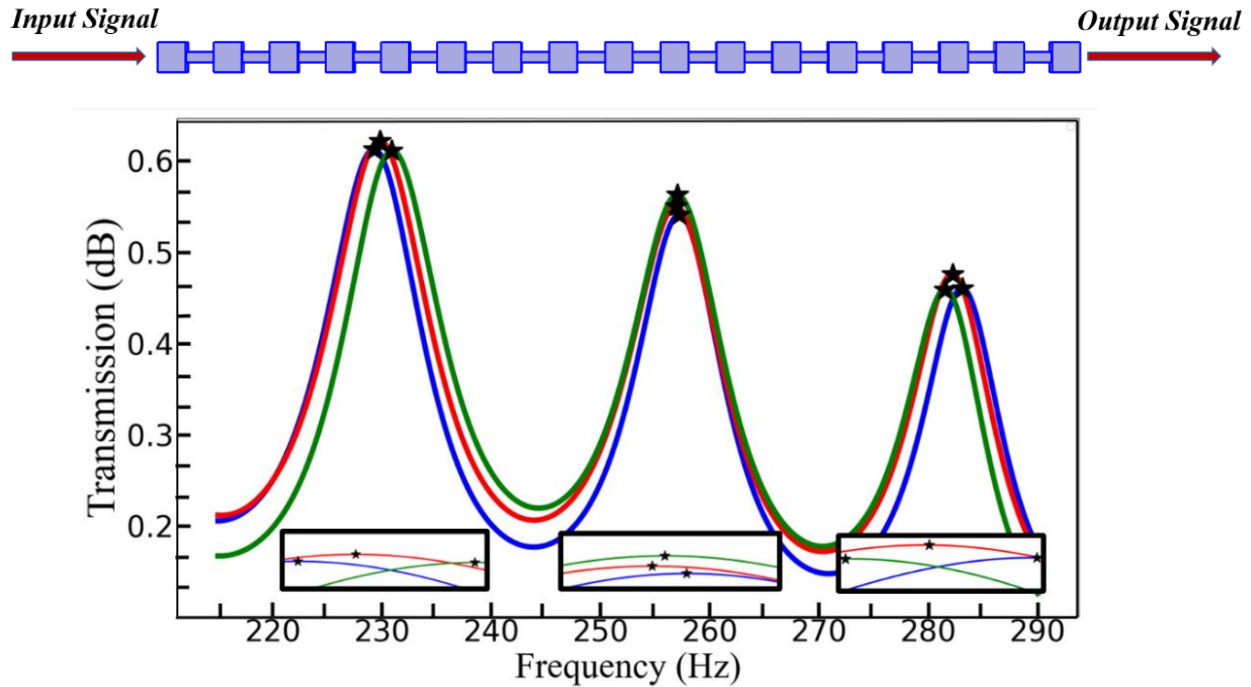
Figure 2. 4: Full-wave numerical demonstration of topologically protected robust bulk state. The upper panel shows that the incoming signal is sent from left side and the outgoing signal is received as transmitted signal in the right side of the waveguide. The lower panel shows three transmission curves (blue curve is without any disorder and red & green curves corresponds to two disordered cases)and the black starts on the peaks indicates three eigenmodes corresponds to three eigenfrequencies sitting at three peaks, where the peak in the middle is associated with the robust mode. Other two modes are from two eigenfrequencies which are not robust against disorder.

We change the length of the rectangles randomly by 10% to observe how the system responds after applying disorder(Zangeneh-Nejad & Fleury, 2019). It is clearly noticed that eigenfrequency (pointed out using red stars) for the second peak fluctuate negligibly in

18

comparison to the 1ˢᵗ and 3ʳᵈ peaks. This is because the second peak corresponds to the topologically robust bulk state and the first and third peaks correspond to some random eigenfrequencies which are not robust. So, we proved numerically with simulation what we have been claiming since the beginning.

2.6 Experimental observation for topologically robust bulk state:

In [Figure 2.5(upper panel)] we can see the experimental setup for topologically robust bulk state. We fabricate a prototype of our acoustic model to verify the topological robustness of the bulk state. In our experimental sample we used polystyrene foam sheets (with density 1050 kg/m³ and bulk modulus 16.5 MPa) with an average thickness of 5mm. The inner cross section of the waveguide along the cuboids is kept 49 cm² and along the rectangles it is kept 5.29 cm². We perform our experiment on the waveguide by sending a signal in a similar way that is shown in the upper panel of [Figure 2.4]. First, we perform the experiment on a waveguide without any disorder in the lattice and collect the data for the outgoing transmitted signal for a range of frequency 215 Hz to 290 Hz. We use a step size of 0.1 Hz to get a precise transmission curve. In [Figure 2.5(lower panel)], the blue dotted curve demonstrates the transmitted spectrum for the system without disorder and the red and green dotted curves corresponds to the disordered system. The stars (black color) indicates the eigenfrequencies at the peak. Following our numerical simulation, we also apply here 10% disorder(Zangeneh-Nejad & Fleury, 2019) in the length of the rectangles and observe that around the frequency 257 Hz (the middle peak of [Figure 2.5]) we see less fluctuation in comparison to another two peaks around 230 Hz and 280 Hz. This indicates that our proposed system is topologically protected against any defect or

19

disorder around the eigenfrequency 257 Hz. This eigenfrequency may vary depending on the size of the system as well as the amount of loss in the system.
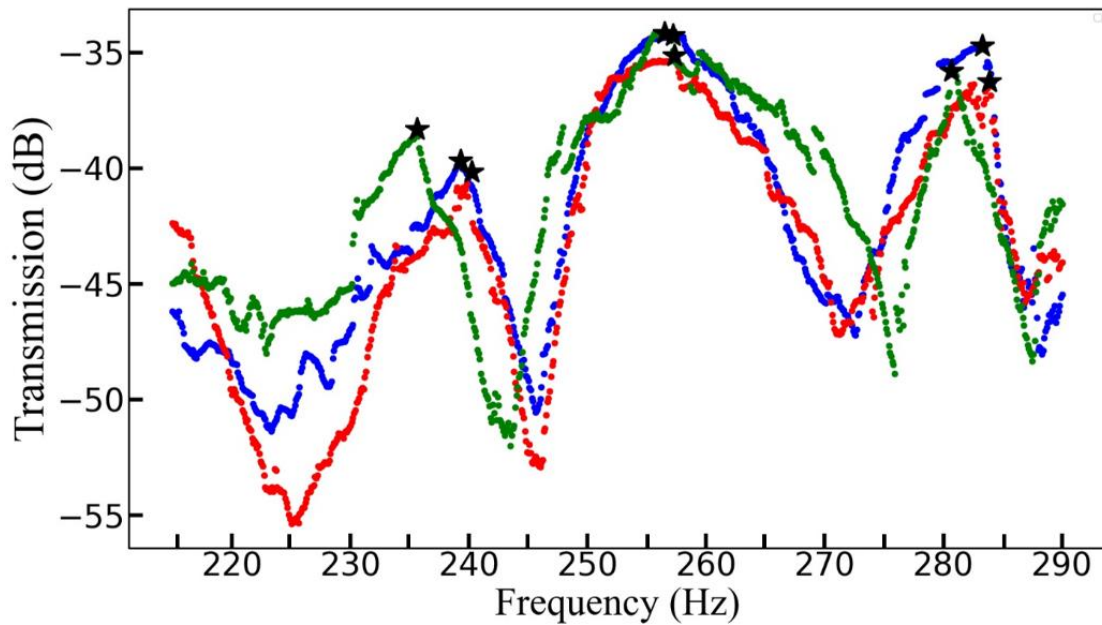
Figure 2.5: Experimental verification of topologically robust bulk state. Upper panel, Experimental setup for robust bulk state. Lower panel, the transmission spectrum for the system without disorder is displayed by the blue curve and for the system with disorder is displayed by the red curve. Topologically robust bulk state is observed around frequency 257 Hz.

But, in every case we will observe topological robustness and the eigenfrequency always stays in the band, not in the gap (same as [Figure 2.3 (b)]).

2.7 Summary:

To conclude the discussions, we have demonstrated theoretically and numerically that it is possible to obtain a 1D lattice in which we observe topologically protected bulk state for a particular mode, not only in Hermitian system but also in a non-Hermitian one. We also have validated our theoretical and numerical finding through experimental observation. We believe that the concept of topologically robust bulk state will offer new perspectives not only in phononics but also in photonics and in other applicative fields. Our results provide a route for developing a new device where direct undisturbed transport of signals is possible.

CHAPTER III

EXPERIMENTAL VERIFICATION OF NUMERICAL RESULTS FOR TUNABLE NON-HERMITIAN ACOUSTIC FILTER

We propose a non-Hermitian acoustic system which is a waveguide and a combination of two types of sub-lattice, the first one is Hermitian sub-lattice and the second is non-Hermitian sub-lattice. In the second sub-lattice adjusting the amount of non-Hermiticity we can tune the acoustic filter in such a way that only certain frequencies will be reflected, and others will be removed from the reflected field. Thus, we will be able to tune the acoustic filter. In this chapter, we will demonstrate the experimental verification of our numerical findings regarding the tunable non-Hermitian acoustic filter.

3.1 Realistic model for tunable non-Hermitian acoustic filter:

To demonstrate our proposed model experimentally, we design the tunable acoustic filter [Figure 3.1]. We fabricate a structure with 4 square passive Hermitian hollow cuboids with $7 \times 7 \times 7$ cm^3 volume and 4 hollow active non-Hermitian hollow cuboids of volume $9.3 \times 9.3 \times 9.3$ cm^3. These cuboids are connected to each other by the rectangular cuboids with $7 \times 2.3 \times 2.3$ cm^3 volume.

The structure was printed using MakerBot Replicator Z18(*Replicator Z18 Professional 3D Printer*, n.d.) with extruded Polylactic Acid (PLA) of density, $\rho = 1190 \text{kg/m}^3$ and Bulk modulus, $\varepsilon = 1.01 \times 10^5$ Pa. We framed square holes with sides (s = 4.6 cm) in the side walls of the large cuboids. We introduced loss as an absorption in the system by placing polystyrene foams in the square holes.
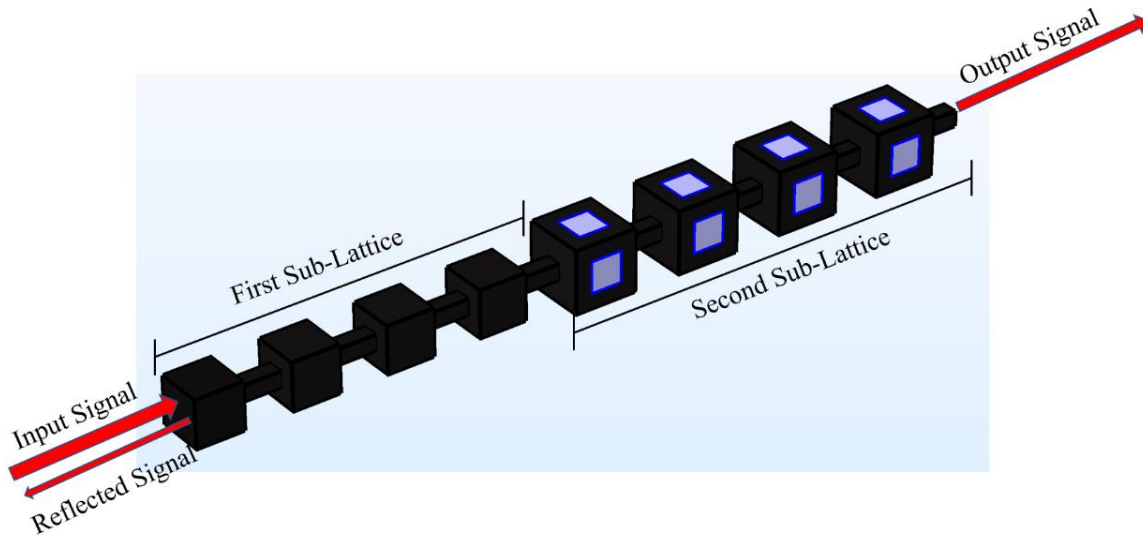
Figure 3. 1: Schematic of the supper-lattice (upper panel) made of two sub-lattices and works as a tunable acoustic filter.

3.2 Experimental set up and introducing non-Hermiticity in the system:

Figure 3. 2: Experimental set up for tunable acoustic filter with the realistic model built using 3d printer.

The experimental set up comprises a loudspeaker connected to [Figure 3.2] a continuous wave 15MHz synthesized function generator, used to generate a continuous acoustic signal inside the waveguide. We captured the acoustic signals using 1/4" omni-directional microphones. We connect the microphones with network analyzer via constant Current power supply to send a low impedance signal to the network analyzer. To introduce the loss we covered the holes with absorbing Polyester foam material which is acting as a loss in the system and we call it non-Hermitian case and in the Hermitian case we cover the holes with leads made of PLA (Polylactic acid) material to make a sound hard boundary wall without absorption(Zangeneh-Nejad & Fleury, 2019).

We perform our scattering experiment for both the non-Hermitian and Hermitian structures where we measure the reflection in a homemade anechoic chamber. To measure reflection is a bit tricky where we used two different waveguides, to measure input signal and (input + reflected) signal respectively and subtract them to get only reflected signal. The wave guide which we used to measure only the input signal is with high absorption where the walls are sound soft boundary walls to avoid reflection and we put the microphone at the beginning of the waveguide and measure the input signal amplitude in the network analyzer. We used our proposed tunable acoustic filter to measure (input + reflected) signal similarly placing the microphone at the beginning of the waveguide, where we can get the reflection as the walls are sound hard boundary walls.

3.3 Comparison of experimental data with the simulation:

We observe the spectrum of our acoustic wave in the network analyzer from where we extract our data. To calculate the reflected amplitude, we used the formula for decibel

Loudness in $dB = 10 \times log_{10} \times \frac{I'}{I_0}$

where $I_0 = 10^{12}$ W/m^2 is the standard intensity and I' is the measured intensity(*Decibels*, n.d.).

In [Figure 3.3] we presented the experimental reflection (blue curve) and the corresponding simulation (red dotted curve) for non-Hermitian case, with effective model and a = 0.2 in panel a, and Hermitian case in panel b for a = 0. Here, for both panels we consider 0 dB as our reference input which is along the baseline outside of the resonance dips(Sheng & Lue, 1992) where we notice very high reflection close to 0 dB.

25
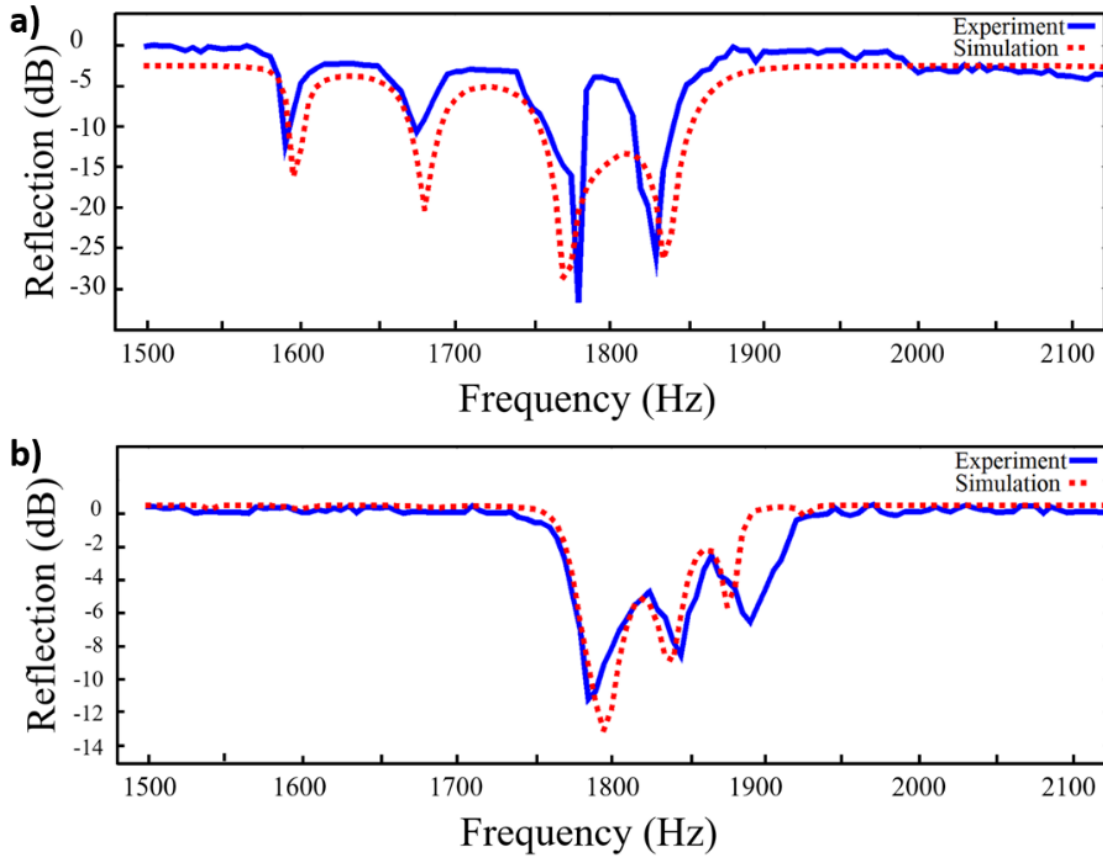
Figure 3. 3: Experimental realization of the tunable acoustic filter. (a) Reflection amplitude for a system with loss embedded in the system. In the experiment (blue solid curve) absorption is induced via holes that are covered by absorbing materials while in the simulation (red dotted curve) we used the effective model with loss parameter a = 0.2. (b) Reflection amplitude for a system without loss, namely no hole in the cuboids. We observe that in the band gap two dips are appearing when loss is induced in the system.

We observe a nice agreement between simulation and experimental data. The experimental data nicely depicts the filtering phenomenon that we predicted. Furthermore, our experimental data agrees well with the effective model in this frequency range. Notice that by increasing the number of cuboids in the Hermitian part one can induce more resonances (as shown in our simulations) and thus remove other frequencies from the reflected field(Zangeneh-Nejad & Fleury, 2019).

3.4 Summary:

In this chapter we discuss the experimental verification of the theoretical and numerical findings for tunable non-Hermitian phononic/acoustic filter(*001.Pdf*, n.d.) which is an accumulation of two sublattices (Hermitian and non-Hermitian sublattice). We showed that depending on the amount of applied loss in the non-Hermitian sub-lattice we can locally control the tunability, resonance phenomena as well as the reflected wave at will.

CHAPTER IV

METHOD AND MATERIALS FOR EXPERIMENT IN ACOUSTIC LAB

This chapter discusses the basic methods that we employ to use devices to build the sample structure and to perform experiment. We will explain the steps followed for simulation to build the geometry of the structure, to find the band structure, and to find the transmission and reflection spectra. We will describe the techniques used to analyze the data that we extract and data analysis process for different scattering experiments.

4.1 Simulation:

4.1.1   Finding Band structure in COMSOL

As our waveguide is a periodic spring mass lattice according to Bloch's theorem explained in chapter I, the wave function of the acoustic signal inside the waveguide is

$$\psi(\mathrm{x}) = e^{ikx}\, u_k(x)$$

The exponent k is called the wavenumber. The wavenumber has several properties. First, the set of solutions remain the same if we shift $k \rightarrow k + 2\pi/a$ so the wavenumber takes values in

$$k \in [\frac{-\pi}{a}, \frac{\pi}{a}]$$

This range of k is named as Brillouin zone. In COMSOL MULTIPHYSICS using the idea o

irreducible Brillouin zone and using if conditions we can find the band structure for a unit cell of a periodic lattice. To do that let us consider a unit cell:
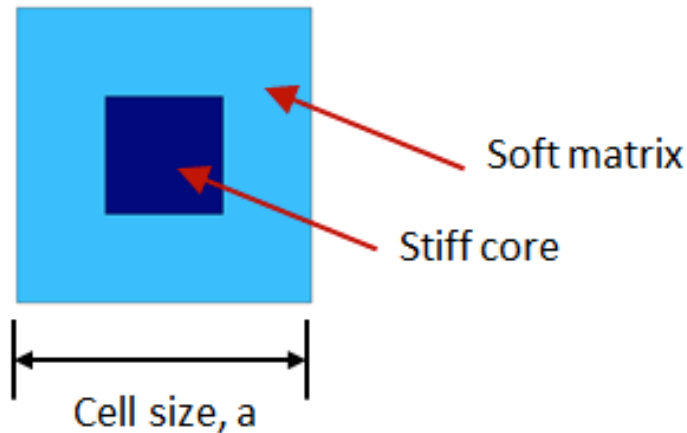
Figure 4. 1: A schematic of a unit cell of a phononic crystal. The cell is composed of a stiff core material and a softer outer matrix material.

By analyzing the periodic unit cell [Figure 4.1] we can evaluate the frequency response of a phononic crystal using Bloch's periodic boundary conditions spanning the wave vector, k. Then we span the a relatively small range of wave vectors covering the edges of the irreducible Brillouin zone (IBZ). For rectangular 2D structures, the IBZ (shown below) spans from Γ to X to M (k_x) and then back to Γ (k_y). Even for a 3D structure if the motion of the wave is 2 dimensional, it is enough to span the wave vectors along k_x and k_y.
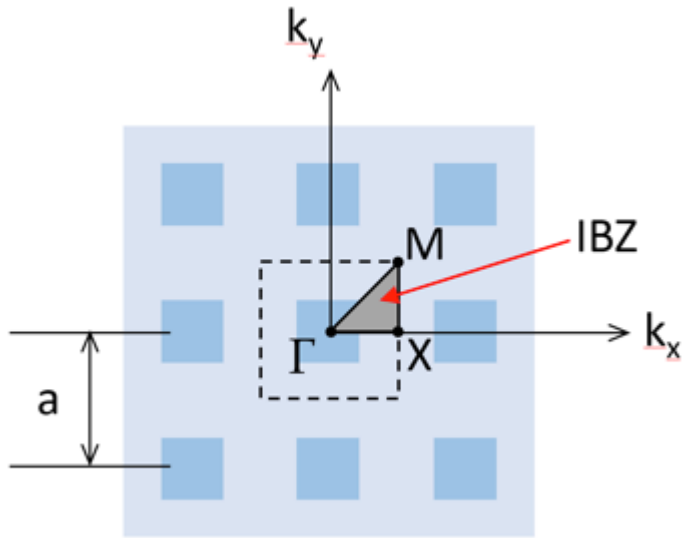
Figure 4. 2: The irreducible Brillouin zone for 2D square periodic structures.

In COMSOL Multiphysics, the Bloch's boundary conditions are known as the Floquet boundary conditions in 1D to constrain the boundary displacements of the periodic structure defined by the following formula,

$$u_{destination} = exp\left[-i\mathbf{k}_F \cdot \left(r_{destination} - r_{source}\right)\right]u_{source}$$

Where $k = k_F$ = wave vector.

In the unit cell we need to apply source and destination two times. For k_x to the left and right edges and for k_y to the top and bottom edges which is considered to be the boundary condition.

Here, $k_x = 2\pi/a$, in x direction

$k_y = 2\pi/a$, in y direction

To find the band structure we do the eigenfrequency analysis as a parametric sweep involving one parameter, k, which varies from 0 to 3. Here, 0 to 1 defines a wave number spanning the Γ-X edge, 1 to 2 defines a wave number spanning the X-M edge, and 2 to 3 defines a wave number spanning the diagonal M-Γ edge of the IBZ.[Figure 4.2] for each k parameter, we solve for the lowest natural frequencies. We sweep parameter k from 0 to 3 using the following if condition.

For the irreducible Brillouin zone,

From Γ-X edge: $k_x = [0, \pi/a]$ and $k_y = 0$

From X-M edge: $k_x = \pi/a$ and $k_y = [0, \pi/a]$

From M-Γ edge: $k_x = [\pi/a, 0]$ and $k_y = [\pi/a, 0]$

Now relating parameter k with k_x and k_y:

$$
k_x = \begin{cases}
k * (\pi/a) & \text{if } 0 < k < 1 \\
\pi/a & \text{if } 1 < k < 2 \\
(3-k) * \pi/a & \text{if } 2 < k < 3
\end{cases}
$$

$$
k_y = \begin{cases}
0 & \text{if } 0 < k < 1 \\
(k-1) * \pi/a & \text{if } 1 < k < 2 \\
(3-k) * \pi/a & \text{if } 2 < k < 3
\end{cases}
$$

In COMSOL these conditions can be used as if condition like below:

k_x= if (k<1,pi/L1*k, if(k<2,pi/L1, (3-k)*pi/L1))

k_y= if (k<1,0,if(k<2, (k-1)*pi/L1, (3-k)*pi/L1))

Then we plot the wave propagation frequencies for each value of *k* and get the band diagram("Modeling Phononic Band Gap Materials and Structures," n.d.) like [Figure 4.3] for a unit cell size of 1 cm × 1 cm and a core material size of 4 mm × 4 mm with Bulk modulus of 2 GPa and a density of 1000 kg/m³. In the range of frequency(f) 60 kHz to 72 kHz we observe the band gap where we expect reflection and in rest of the frequency range, we observe bands where we expect transmission.

Similarly in Figure 2.3 (b) we see the band diagram/structure for the proposed periodic acoustic lattice where we observed robust extended bulk state where we sweep parameter *k* from -1 to 1 for the frequency range 0 to 400 Hz and here we do not see any band gap in the diagram. It indicates a reflection free transmission for these particular k and f values and getting this information from band structure we decided to get the transmission spectrum through COMSOL simulation to verify the robustness of our spring mass lattice.
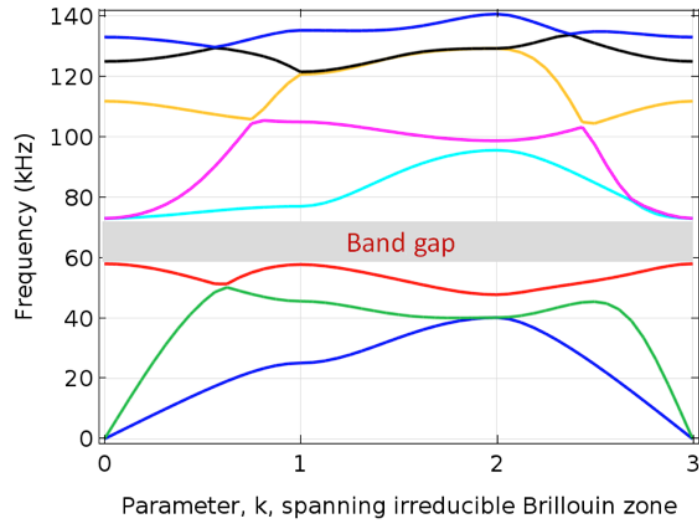
Figure 4. 3: The frequency band diagram for selected unit cell parameters.

4.1.2   Finding Transmission and Reflection spectra in COMSOL

We have seen that while finding the band structure, we take one-unit cell of a periodic lattice to get the band structure. But to get the transmission spectrum we need to take the whole truncated periodic structure to observe its topological aspect and to get the transmission spectrum. In COMSOL Multiphysics we can study both Frequency domain analysis and Eigenfrequency analysis of a structure. To get different eigenfrequencies we do the eigenfrequency analysis and to get transmission spectrum we do the frequency domain analysis.

In the second type of analysis we need to choose a 1D plot Group and then choose Global plot type. In the settings of the Global for Expression of y-Axis Data we can choose two scattering parameters, abs(acpr.S21)^2 for transmission and abs(acpr.S11)^2 for reflection, and along x-axis are the frequencies. So, we used the first expression of scattering parameters to plot the transmission spectrum. [Figure 2.4 (lower panel)] is the transmission spectrum (Percentage of

33

transmission vs Frequency using Global plot type). [Figure 3.3 (a, b)] are the reflection

spectrums (Reflection in decibel vs Frequency using Octave band plot type). If we look at the

acoustic pressure field section, we can observe the pressure field for each frequency depending

on the step size in the frequency domain of the study(*Transmission in Duct with Right-Angled*

Bend, n.d.).

4.2 Experiment:

4.2.1   Building Model using 3d Printer:

We fabricate our tunable non-Hermitian acoustic filter using 3d printer. Below is explained

the whole procedure of modeling our structure using 3D printer.

4.2.1.1 **Routing Filament and loading filament:**

The 3d printer that we used is MakerBot Replicator z18(*Replicator Z18 Professional 3D*

Printer, n.d.). After unpacking it and setting up and placing the polylactic acid filament spool in

the drawer we detach the free end of the filament from the spool and insert it into the hole at the

back-left corner of the filament drawer. Then we continue to feed the filament by hand into the

slot at the side of the filament drawer. The filament will move up through the MakerBot

Replicator Z18 to the top compartment. We stop feeding the filament when we see it emerging

from the end of the filament guide tube. Then we apply the build plate where the sample will be

built and then plug and power on.

When instructed to by the LCD screen, we press the control panel dial to start heating the

extruder. After the extruder is fully heated, we push the free end of the filament into the loading

tube. Then we keep pushing on the filament until you feel the extruder pulling it in. We wait

until you begin to see plastic emerging from the extruder nozzle. Then we press the control panel

dial to stop extrusion. Then the printer is ready to print an object(*Z18_user_manual-1.Pdf*, n.d.).

4.2.1.2 **Process of printing an object:**

Below is explained step by step how the 3D printing was done. It includes the use of several

others devices other than the 3D printer.

Printing test object: There are some loaded STL files in the internal storage of printer. As a

starter it is better to do a test printing using those files. After the printing is finished, we need to

remove it from the build surface.

Connecting to the computer: Now, if we want to move a file from a computer to MakerBot

Replicator Z18, there are four ways to do that: Wi-Fi, Ethernet, USB cable and USB drive. We

follow the third way and connect the computer to the printer via USB cable.

Downloading, installing, and using MakerBot desktop: We open a browser session and go

to makerbot.com/desktop and download and install it from there. When we are ready to print, we

just need to open the STL file of the object in the MakerBot Desktop we want to print. There we

can select any model and units for that model. We can also arrange the model on the build plate

customize its density, support thickness and scale it at any size so that we can place it in the build

plate.

Designing 3d object: We design our own model using COMSOL MULTIPHYSICS and

then convert the mph file into an STL file. It is also possible to use other 3d designing software

like Blender, AutoCAD etc. to design 3d object. In every case we need to convert the files into

STL to use it for 3D printing.

4.2.2 Building Model manually

As 3d printing is a very time-consuming process, we later build the acoustic lattice structure for the observation of robust bulk state using polyester foam sheet. We first cut the squares and rectangular sides and glued the parts using glue gun and build the whole structure in completely homemade way. As 3D printing is time consuming, we think making the structure manually saves time. Though because of using polyester-foam sheet instead of polylactic acid we introduce loss in the system, it can be compensated changing some parameters in the simulation (*3d Printing Using Makerbot Replicator Z18 - YouTube*, n.d.).

4.2.3 Instructions for using devices in Experimental Setup:

For the experimental set up we use several devices which are explained below.

Function Generator: A function generation can produce different types of wave/signals (sine wave, square wave, triangular wave, or sawtooth wave) of different amplitudes and frequencies. We use BNC cables and crocodile clips to connect the output of the function generator with the loudspeaker to produce an acoustic signal. For our experiment we used DS340 15 MHz Synthesized Function Generator. Generally, we fix a single frequency to generate the signal. We can also sweep the frequency of a fixed range with specific sweeping rate which helps to understand where we can observe a resonance within that range. In sweep mode, the function generator outputs a single sweep when a trigger signal is received. After one sweep from the start frequency to the stop frequency, it waits for the next trigger while outputting the start frequency(*DS340m.Pdf*, n.d.).

Microphones and signal conditioner: We used Bruel & Kjaer $1/4''$ omnidirectional microphones(*Type 4944 1/4" Pressure-Field Microphone | Brüel & Kjær*, n.d.). Because of being omni directional it is very sensitive to the signal and can capture sound from all direction. To get transmission data we place a microphone at the end of the waveguide and to get reflection data we place to microphone at the beginning of the wave guide. We connect the microphones with a Bruel & Kjaer 1704 Battery Powered CCLD Signal Conditioner(*Signal Conditioner | Type 1704 | Brüel & Kjær*, n.d.) to get a low impedance signal which also act as an amplifier. This signal conditioner amplifies the signal from the microphone and then send it to the signal analyzer.

Network Analyzer: The signal conditioner is connected to the SR770 FFT network analyzer where we observe the Amplitude vs frequency spectrum. We use auto scale or auto range, but if we focus on a particular frequency range, we can set up the range using frequency span. We can also scale the screen for our convenience. To read the maximum/minimum amplitude we need to press the Max/Min key under Marker. We can extract data both manually and through USB drive. If we need data for a single frequency it is better to get spectrum with USB drive using the storage key under Menu. As we needed to find the transmission and reflection spectrum for a frequency range, we took the data manually(*SR770m.Pdf*, n.d.).

4.3 Extracting data for the Scattering experiment:

We perform two types of Scattering experiment on our system, transmission, and reflection. For Transmission we can directly take the amplitudes of the signal from the end of the waveguide keeping that end open to avoid reflection. In But while taking reflection data we need to be tricky and first pass the signal through a wave guide with sound soft boundary wall so

that if we put the microphone at the beginning of the waveguide we can only receive the incoming signal (let us call it first data) avoiding reflection. Then we take the data putting the microphone at the beginning of our structure to receive both incoming and reflected signal (there will be reflection because of the sound hard boundary wall and let us call it second data). Then we subtract the 2nd data from the 1st one by considering the incoming signal as our reference level. After the subtraction we find the reflected signal amplitudes. That is how we extract data for scattering experiment, that is transmission and reflection.

CHAPTER V

CONCLUSION

In conclusions, we would like to summarize the main points of our work with some remarks on the results. We will summarize the purpose of each chapter.

In the 1st chapter we explained the basics of Hermitian and non-Hermitian systems, topology, Bloch's theorem, and spring mass model which are needed to know to understand our work.

In the 2nd chapter we show that in a spring mass system associated with a noninvertible Hamiltonian, it is possible to have topologically robust bulk state, which is not localized but extended. In acoustics this allows direct transport of acoustic signal through the bulk, in electronics it allows electrons conduction through the bulk. We report simulation and experimental verification of such robust bulk state in our proposed acoustic system, where this robust state holds not only for the Hermitian system but also for the non-Hermitian one.

The 3rd chapter is based on the non-Hermitian tunable acoustic filter. Here we discussed the experimental procedure and results and compare the results with simulation.

In the 4th chapter we explained how we build the band structure and scattering parameters in COMSOL Multiphysics as well as the methodologies of building sample and using devices.

REFRENCES

001.pdf. (n.d.). Retrieved May 7, 2021, from

https://www.blackwellpublishing.com/content/BPL_Images/Content_store/Sample_chapt

er/9781405101233/001.pdf

3d printing using makerbot replicator z18—YouTube. (n.d.). Retrieved May 7, 2021, from

https://www.youtube.com/

Acoustic metamaterial. (2021). In *Wikipedia*.

https://en.wikipedia.org/w/index.php?title=Acoustic_metamaterial&oldid=1021830173

Al Jahdali, R., & Wu, Y. (2018). Coupled Resonators for Sound Trapping and Absorption.

Scientific Reports, *8*(1), 13855. https://doi.org/10.1038/s41598-018-32135-5

Ashida, Y., Gong, Z., & Ueda, M. (2020). Non-Hermitian Physics. *Advances in Physics*, *69*(3),

249–435. https://doi.org/10.1080/00018732.2021.1876991

Bender, C. M. (2007). Making Sense of Non-Hermitian Hamiltonians. *Reports on Progress in

Physics*, *70*(6), 947–1018. https://doi.org/10.1088/0034-4885/70/6/R03

Billie Eilish. (2015, June 30). *Intro to Topology*. https://www.youtube.com/watch?v=C-

eJW0gEm5w

C. Yuce. (n.d.). Robust bulk states | Elsevier enhanced reader. *Physics Letters A*, *383*, 1791–
   1794. https://doi.org/10.1016/j.physleta.2019.02.040

COMSOL: Multiphysics Software for Optimizing Designs. (n.d.). COMSOL. Retrieved May 7,
   2021, from https://www.comsol.com/

Decibels. (n.d.). Retrieved May 7, 2021, from http://hyperphysics.phy-
   astr.gsu.edu/hbase/Sound/db.html

DS340m.pdf. (n.d.). Retrieved May 7, 2021, from
   https://www.thinksrs.com/downloads/pdfs/manuals/DS340m.pdf

Gao, H., Xue, H., Wang, Q., Gu, Z., Liu, T., Zhu, J., & Zhang, B. (2020). Observation of
   topological edge states induced solely by non-Hermiticity in an acoustic crystal. *Physical
   Review B*, *101*(18), 180303. https://doi.org/10.1103/PhysRevB.101.180303

Hasan, M. Z., & Kane, C. L. (2010). Topological Insulators. *Reviews of Modern Physics*, *82*(4),
   3045–3067. https://doi.org/10.1103/RevModPhys.82.3045

Jamuna TV. (2019, May 29). *Bloch's Theorem in Crystals*.
   https://www.youtube.com/watch?v=8EOReuCrNuE

Modeling Phononic Band Gap Materials and Structures. (n.d.). *COMSOL Multiphysics*.
   Retrieved May 7, 2021, from https://www.comsol.com/blogs/modeling-phononic-band-
   gap-materials-and-structures/

Moessner, R., & Moore, J. E. (2021). *Topological Phases of Matter*. Cambridge University
   Press. https://doi.org/10.1017/9781316226308

Qi, X.-L., & Zhang, S.-C. (2011). Topological insulators and superconductors. *Reviews of
   Modern Physics*, *83*(4), 1057–1110. https://doi.org/10.1103/RevModPhys.83.1057

Quantum Harmonic Oscillator. (n.d.). Retrieved May 7, 2021, from http://hyperphysics.phy-

    astr.gsu.edu/hbase/quantum/hosc2.html

Ramezani, H., Christodoulides, D. N., Kovanis, V., Vitebskiy, I., & Kottos, T. (2012). P T-

    symmetric Talbot effects. *Physical Review Letters*, *109*(3), 033902.

Replicator Z18 Professional 3D Printer. (n.d.). MakerBot. Retrieved May 7, 2021, from

    https://www.makerbot.com/3d-printers/replicator-z18/

Rivero, J. D. H., & Ge, L. (2020). Origin of robust exceptional points: A restricted bulk zero

    mode. *Physical Review A*, *101*(6), 063823.

    https://doi.org/10.1103/PhysRevA.101.063823

Schindler, J., Lin, Z., Lee, J. M., Ramezani, H., Ellis, F. M., & Kottos, T. (2012).

    \textdollar\textbackslashmathcal$\lbrace$PT$\rbrace$\textdollar-symmetric electronics.

    Journal of Physics A: Mathematical and Theoretical, *45*(44), 444029.

    https://doi.org/10.1088/1751-8113/45/44/444029

Sheng, J.-S., & Lue, J.-T. (1992). Resonant reflectance dips induced by coupled surface plasmon

    polaritons in thin metal-film/dielectric superlattices. *Applied Physics A*, *55*(6), 537–544.

    https://doi.org/10.1007/BF00331670

Shulman, H., & Prodan, E. (2010). Robust extended states in a topological bulk model with even

    spin-Chern invariant. *ArXiv:1011.5456 [Cond-Mat, Physics:Math-Ph]*.

    http://arxiv.org/abs/1011.5456

Signal Conditioner | Type 1704 | Brüel & Kjær. (n.d.). Retrieved May 7, 2021, from

    https://www.bksv.com/en/transducers/signal-conditioning/ccld/1704-a-002

SR770m.pdf. (n.d.). Retrieved May 7, 2021, from

    https://www.thinksrs.com/downloads/pdfs/manuals/SR770m.pdf

Svela, A. Ø., Silver, J. M., Del Bino, L., Zhang, S., Woodley, M. T. M., Vanner, M. R., &
Del'Haye, P. (2020). Coherent suppression of backscattering in optical microresonators.
Light: Science & Applications, *9*(1), 204. https://doi.org/10.1038/s41377-020-00440-2

Thorton & MArion. (n.d.). *Classical Dynamics of Particles and Systems, 5th Edition—Cengage*
(5th ed.). Thomson Brooks. Retrieved May 7, 2021, from /c/classical-dynamics-of-
particles-and-systems-5e-thornton/9780534408961PF

Topology in physics. (n.d.). Retrieved May 7, 2021, from https://www.quora.com/What-is-
topology-in-maths-and-physics

Transmission in Duct with Right-Angled Bend. (n.d.). COMSOL. Retrieved May 7, 2021, from
https://www.comsol.com/model/duct-with-right-angled-bend-67601

Type 4944 1/4" Pressure-Field Microphone | Brüel & Kjær. (n.d.). Retrieved May 7, 2021, from
https://www.bksv.com/en/transducers/acoustic/microphones/microphone-cartridges/4944

Witte, C. (2009). Hamiltonian Operator. In D. Greenberger, K. Hentschel, & F. Weinert (Eds.),
Compendium of Quantum Physics (pp. 271–275). Springer. https://doi.org/10.1007/978-
3-540-70626-7_82

Yang, Z., Gao, F., Shi, X., Lin, X., Gao, Z., Chong, Y., & Zhang, B. (2015). Topological
Acoustics. *Physical Review Letters*, *114*(11), 114301.
https://doi.org/10.1103/PhysRevLett.114.114301

Z18_user_manual-1.pdf. (n.d.). Retrieved May 7, 2021, from http://www.makerbot.com/wp-
content/uploads/2018/09/z18_user_manual-1.pdf

Zangeneh-Nejad, F., & Fleury, R. (2019). Topological Fano Resonances. *Physical Review
Letters*, *122*(1), 014301. https://doi.org/10.1103/PhysRevLett.122.014301

Zhao, W., Jiang, H., Liu, B., Jiang, Y., Tang, C., & Li, J. (2015). Fano resonance based optical modulator reaching 85% modulation depth. *Applied Physics Letters*, *107*(17), 171109. https://doi.org/10.1063/1.4935031

BIOGRAPHICAL SKETCH

Jannatul Ferdous was born on 1st July,1992 in Comilla, Chittagong, Bangladesh. She earned her Bachelor of Science degree in physics and Master of Science degree in physics from the University of Dhaka, Bangladesh in 2014 and 2016, respectively. She was awarded her second Master of Science in Physics degree from the University of Texas Rio Grande Valley in May 2021. Her personal email address is jannatultroee@gmail.com.